Journal of Molecular Structure 1321 (2025) 139964

Contents lists available at ScienceDirect

Journal of Molecular Structure

journal homepage: www.elsevier.com/locate/molstr

Complexes exhibiting *trans*(Cl)-$RuCl_2$(dmso-*S*)$_2$ geometry with methyl-picolinate-type neutral *N,O*-ligands: Synthesis, structural characterization, and chemical behavior analysis in aqueous solutions

Mari Toyama [a,b,c,*], Yuto Onishi [b], Nobuyoshi Tanaka [c], Noriharu Nagao [c]

[a] Research Center for Safe Nuclear System, Institute for Integrated Radiation and Nuclear Science, Kyoto University, 2-1010 Asashiro Nishi, Kumatori 590-0494, Osaka, Japan
[b] Department of Engineering Science, Faculty of Engineering, Osaka Electro-Communication University, 18-8 Hatsucho, Neyagawa, 572-8530, Osaka, Japan
[c] Department of Applied Chemistry, School of Science and Technology, Meiji University, 1-1-1 Higashimita, Kawasaki 214-8571, Kanagawa, Japan

ARTICLE INFO

Keywords:
Ruthenium(II) complex
Hemilabile *N,O*-ligand
2-picolinic acid methyl ether
X-ray crystal structure
NMR spectroscopy
Absorption spectroscopy

ABSTRACT

Methyl picolinate (Mepic) is a starting material in the synthesis of several organic materials and enzymes. Notably, Mepic-ligand-based complexes with metals such as Zn(II), Cd(II), Ru(II), and Rh(III) have garnered attention for catalysis; however, Ru(II)–Mepic complexes remain structurally unexplored. In this study, *trans*(Cl)-[$RuCl_2$(dmso-*S*)$_2$(Mepic)]·0·25H_2O (**1**·0·25H_2O, dmso = dimethyl sulfoxide) was produced in a satisfactory yield (80%) via the reaction of *trans*(Cl)-[$RuCl_2$(dmso-*S*)$_4$] with neutral *N,O*-ligand Mepic in methanol (MeOH) at room temperature. The use of picolinic acid (Hpic) instead of Mepic in H_2O-ethanol (EtOH) produced the corresponding complex—*trans*(Cl)-[$RuCl_2$(dmso-*S*)$_2$(Hpic)]·H_2O (**2**·H_2O)—with a slightly higher yield (82%). Crystal structure analysis of **1**·0·25H_2O and **2**·H_2O revealed that each chelating ligand coordinated to Ru^{2+} *via* pyridyl-*N* and carbonyl-*O* atoms and Hpic acted as a neutral bidentate ligand in **2**. In DMSO, **1** was labile and released Mepic to form [$RuCl_2$(dmso)$_4$], owing to the hemilability of *N,O*-ligand Mepic. In contrast, **2** was inert in DMSO because H^+ was released from Hpic in solution, forming the anionic mono(pic)Ru complex—*trans*(Cl)-[$RuCl_2$(dmso-*S*)$_2$(pic-κ^2*N,O*$^-$)]$^-$. ^{1}H NMR and UV–Vis spectroscopic studies showed that **2** also generated the anionic mono(pic)Ru complex in aqueous solutions. Although free Mepic is inert in water, **1** underwent thermal hydrolysis in water to produce free MeOH. The dissociation of monodentate ligands was also observed in the thermal hydrolysis of **1**. Thus, it was a complicated reaction. The reaction of **1** with equimolar OH^- in water quickly and selectively yielded the same complex and a MeOH molecule. Our study will assist in assessing the catalytic potential of this complex and related systems.

1. Introduction

2-Pyridinecarboxylic acid, methyl ester or methyl picolinate (Mepic; Fig. 1a) can be synthesized *via* metal-catalyzed esterification by the oxidation of primary pyridine alcohols or alkoxycarbonylation with pyridine iodide, primary alcohols, and carbon monoxide [1–3]. Mepic has been used as a starting material for amidation- or nitration-based organic synthesis and enzymatic synthesis [4–7]. M(Mepic) complexes (M = Zn(II), Cd(II), Ru(II), or Rh(III)) have been investigated to clarify the catalytic reaction mechanism between metal ions and Mepic; to our knowledge, four reports have been published on this topic; however, ample opportunity remains for further study [8–11]. Three crystal structures of M(Mepic) complexes (M = Zn(II), Cd(II), or Rh(III)) have been reported, and these structural analyses suggest that Mepic acts as a neutral hemilabile *N,O*-ligand *via* pyridyl-*N* and carbonyl-*O* atoms. However, the crystal structures of Ru(II) complexes with Mepic have not yet been documented [11]. Bidentate chelating hemilabile *N,O*-ligands are more prone to chelate ring-opening reactions than *N,N′*-ligands. In the case of Ru(II) complexes, a Ru(II)-N bond is stronger than a Ru(II)-O bond. Furthermore, neutral ligands have less electronic interaction with the central metal than anionic ligands; thus, ligand desorption from the metal complex is more likely to occur. In summary, the investigation of the structure and reactivity of the complexes with neutral hemilabile *N,O*-ligands will promote the evaluation of their catalytic ability.

2-Acetylpyridine (apy; Fig. 1b), which is structurally similar to Mepic and acts as a neutral hemilabile *N,O*-ligand, is frequently used in

* Corresponding author.
E-mail address: toyama.mari.3p@kyoto-u.ac.jp (M. Toyama).

https://doi.org/10.1016/j.molstruc.2024.139964
Received 27 May 2024; Received in revised form 3 September 2024; Accepted 5 September 2024
Available online 6 September 2024

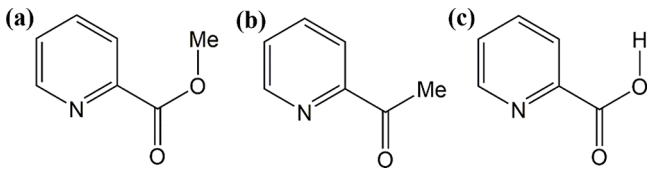

Fig. 1. Structures of (a) Mepic and related neutral *N,O*-ligands, (b) apy and (c) Hpic.

coordination chemistry. Notably, Ru(II) complexes with the apy ligand have been reported [11–15]. Furthermore, picolinic acid (Hpic; Fig. 1c), which is a common ligand in coordination chemistry [16–21], is also structurally similar to Mepic. However, when Hpic is coordinated to a metal ion, the ligand releases a proton and consequently functions as a negative bidentate ligand, pic^-. Furthermore, a Ru(II) complex with neutral Hpic has not yet been reported although Ru(II)-pic^- complexes have been studied.

We previously reported three types of Ru(II) complexes with pyridine-based neutral *N,O*-ligands di-2-pyridyl ketone (dpk), (phenyl) pyridyl ketone (ppk), and 2-picolinamide (H_2pia), which are coordinated to a Ru(II) ion *via* pyridyl-*N* and carbonyl-*O* atoms to form a five-membered chelate ring [22–25]. In particular, *trans*(Cl)-[$RuCl_2$(dmso-*S*)$_2$(dpk-κ^2*N,O*)] (dmso = dimethyl sulfoxide), which is obtained from the reaction of *trans*(Cl)-[$RuCl_2$(dmso-*S*)$_4$] with dpk in H_2O-EtOH at 275 K, reportedly exhibited a unique isomerization reaction on the Ru(II) ion [22]. The dpk-κ^2*N,O* coordination mode thermally isomerized to dpk-κ^2*N,N′*, which coordinates to the Ru^{2+} ion *via* two pyridyl-*N* atoms. Moreover, when the complex with the dpk-κ^2*N,O* ligand reacts with OH^- ions in water at room temperature, the C=O group transforms to negatively charged diol group $C(OH)O^-$, yielding *trans*(Cl,O)-[RuCl(dmso-*S*)$_2$(dpk-OH-κ^3*N,O*$^-$,*N′*)], in which dpk-OH functions as an anionic tridentate ligand.

In this study, a *trans*(Cl)-[$RuCl_2$(dmso-*S*)$_2$(Mepic)]·0·25H_2O complex (**1**·0·25H_2O) was synthesized based on the method used to prepare the aforementioned dpk-κ^2*N,O* complex [22]. In the synthesis of **1**·0·25H_2O, methanol (MeOH) was used as a solvent. MeOH is used as a solvent in the synthesis of several neutral Ru(II) complexes that use *cis*(Cl),*fac*(*S*)-[$RuCl_2$(dmso-*S*)$_3$(dmso-*O*)]—an isomer of *trans*(Cl)-[$RuCl_2$(dmso-*S*)$_4$]—as a starting material [26–28]. Subsequently, the crystal structure and reactivity of this Mepic complex in water were assessed. Additionally, the analogous Ru(II) complex with Hpic was synthesized, and the *trans*(Cl)-[$RuCl_2$(dmso-*S*)$_2$(Hpic)]·H_2O complex (**2**·H_2O) was obtained. The crystal structure study, elemental analysis, and ^{1}H nuclear magnetic resonance (NMR) spectroscopy of **2**·H_2O revealed that Hpic acted as a neutral ligand in **2**. Hpic was not expected to coordinate in a neutral form. Therefore, it is important that the composition is identified by multiple analytical results. To our knowledge, this study is the first on the crystal structures of Ru(II) complexes with Mepic or neutral Hpic as the ligand. Furthermore, the chemical behavior of **1**·0·25H_2O and **2**·H_2O in DMSO and water solutions was investigated by ^{1}H NMR and ultraviolet–visible (UV–Vis) spectroscopy. DMSO is a common solvent for NMR measurements of Ru(II)-dmso complexes because of its high solubility in both neutral and ionic complexes. The dmso ligands of Ru(II)-dmso complexes are often substituted with coordinating solvent molecules. However, with DMSO-d_6, NMR analysis is easy because the chemical structure of the complex does not change if coordinating dmso and solvent DMSO-d_6 are substituted. Moreover, DMSO is a highly coordinative solvent and suitable to evaluate hemilabile *N,O*-ligands. Water was also used because it is the most common solvent. The thermal reaction and pH dependence of **1**·0·25H_2O and **2**·H_2O in water were investigated. Mepic is inert in water; however, MeOH slowly dissociated from **1**·0·25H_2O upon heating in water. Dissociation of the monodentate ligands of **1** also occurred. The reaction of **1** with OH^- ions in water rapidly produced *trans*(Cl)-[$RuCl_2$(dmso-*S*)$_2$(pic-κ^2*N,O*$^-$)]$^-$ and MeOH, without dissociation of the monodentate ligands. This study provides fundamental insight into Mepic complexes and will aid in future research on the catalytic potential of Mepic.

2. Experimental

2.1. General

The starting material, *trans*(Cl)-[$RuCl_2$(dmso-*S*)$_4$], was prepared according to the literature [26]. All reactions were performed in an argon atmosphere at room temperature (approximately 298 K). ^{1}H NMR spectroscopy was performed using DMSO-d_6, acetone-d_6, CD_3OD, and D_2O at 293 K with a Varian Mercury 300 (300 MHz, Agilent Technologies, Santa Clara, CA, USA), JEOL GSX-270 (270 MHz, Tokyo, Japan), or Magritek Spinsolve 60 (60 MHz, Aachen, Germany) spectrometer, unless otherwise noted. Tetramethylsilane (TMS) was used as the internal standard for DMSO-d_6, acetone-d_6, and CD_3OD, whereas DMSO was used as an internal standard for the measurements in D_2O (2.71 ppm) [29]. The aromatic signals in the ^{1}H NMR spectra of the complexes were assigned based on their coupling constants [30]. Absorption spectra were recorded at 298 K using JASCO V-670 (Tokyo, Japan) and Shimadzu UV-2700 instruments (Kyoto, Japan) with MeOH and H_2O and an ALS SEC2020 spectrometer (Tokyo, Japan) with MeCN. Infrared spectra were recorded on a JASCO FT/IR-6100 (Tokyo, Japan) or HORIBA FT-720 (Kyoto, Japan) spectrometer; the samples were prepared as KBr pellets.

X-ray crystallographic analyses of **1**·0·25H_2O and **2**·H_2O were performed at 173 K using a Rigaku Mercury70 diffractometer (Tokyo, Japan) with graphite monochromated Mo–Kα radiation (λ = 0.71,073 Å) and θ values of 2.94°–30.64° The structures were solved using the direct method with the SIR2014 package and then refined using the full-matrix least-square technique [31–34]. All non-hydrogen atoms were refined using anisotropic displacement parameters. The hydrogen atoms of the pyridyl rings and methyl groups were located at positions theoretically calculated using the riding model. For **2**·H_2O, the hydrogen atoms from the OH group of Hpic in the complex were assigned based on a difference Fourier map. The crystallographic data for **1**·0·25H_2O and **2**·H_2O are

Table 1
Crystallographic data for **1**·0·25H_2O and **2**·H_2O.

	1·0·25H_2O	**2**·H_2O
Chemical formula	$RuCl_2S_2C_{11}NO_{4.25}H_{19.5}$	$RuCl_2S_2C_{10}NO_5H_{19}$
Formula weight	469.88	469.36
Temperature (K)	173	173
Crystal dimensions (mm)	0.20 × 0.20 × 0.05	0.20 × 0.15 × 0.04
Color	Light red	Orange
Crystal system	Triclinic	Orthorhombic
Space group	*P-1* (# 2)	*Pccn* (#56)
Lattice parameters		
a (Å)	8.3311(2)	18.7982(4)
b (Å)	8.3509(2)	13.5456(2)
c (Å)	14.0274(4)	13.8647(2)
α (°)	81.196(2)	90
β (°)	85.092(2)	90
γ (°)	66.880(3)	90
V (Å^3)	886.61(4)	3530.41(10)
Z	2	8
$D_{calcd.}$ (g/cm^3)	1.760	1.766
F_{000}	473.00	1888.00
μ(MoKα, cm^{-1})	1.434	1.443
No. of reflections collected	10,596	42,483
Independent reflections	4573	5079
R_{int}	0.0098	0.0341
R indicates [$I > 2\sigma(I)$]	*R*1 = 0.0206, *wR*2 = 0.0227	*R*1 = 0.0250, *wR*2 = 0.0317
R indicates (all data)	*R*1 = 0.0537, *wR*2 = 0.0548	*R*1 = 0.0575, *wR*2 = 0.0602
Goodness of fit (GOF)	1.093	1.052

summarized in Table 1, and selected bond angles are listed in Table 2 (Cambridge Crystallographic Data Center (CCDC) deposition numbers 2344181 and 2344182).

2.2. Synthesis of *trans*(Cl)-[$RuCl_2$(dmso-*S*)$_2$(Mepic)]·0·25H_2O (**1**·0·25H_2O)

A solution of *trans*(Cl)-[$RuCl_2$(dmso-*S*)$_4$] (0.1 mg, 0.85 mmol) in MeOH (30 mL) was heated at 323 K for 20 min. The yellow heterogeneous solution became a deep-yellow homogeneous solution upon forming *trans*(Cl)-[$RuCl_2$(dmso-*S*)$_2$(MeOH)$_2$]. Mepic (120 μL, 1.1 mmol) was added to the homogeneous solution, and the mixture was stirred for 40 h at room temperature; the deep-yellow solution gradually became red. The resulting solution was evaporated to a volume of approximately 10 mL in a vacuum. Subsequently, diethyl ether (25 mL) was added to the concentrated solution, yielding a red precipitate, **1**·0·25H_2O. After cooling in a refrigerator (approximately 280 K) for over 12 h, the red precipitate was washed several times by decantation with a small amount of diethyl ether, collected by filtration, washed with diethyl ether, and dried *in vacuo* (0.31 g, 80%). Red crystals suitable for X-ray crystallography were obtained by the vapor diffusion of diethyl ether into a mixture of **1**·0·25H_2O in 1:1 methanol–acetone. Analytical calculations for crystals ($RuCl_2C_{11}NS_2O_4H_{19}$·0·25$H_2O$): C, 28.11; H, 4.18; and N, 2.98%. Observed: C, 27.86; H, 4.18; and N, 2.90%. Analytical calculations for dried sample ($RuCl_2C_{11}NS_2O_4H_{19}$): C, 28.39; H, 4.12; and N, 3.01%. Observed: C, 28.14; H, 4.09; and N, 3.04%. ^{1}H NMR (300 MHz, acetone-d_6) $\delta = 10.44$ (1H, d, 3 $J = 5.5$ Hz, H-6), 8.33 (1H, d, 3 $J = 7.8$ Hz, H-3), 8.26 (1H, t, 3 $J = 7.7$ Hz, H-4), 7.96 (1H, dd, 3 $J = 7.7$ and 5.5 Hz, H-5), 4.41 (3H, s, Me of Mepic), 3.45 (6H, s, dmso), 3.43 (6H, s, dmso), and 3.45 (6H, s, dmso). Electronic spectroscopic data in H_2O (nm, $M^{-1}cm^{-1}$): 268 (6.7×10^3), 310 (1.1×10^3), and 395 (1.5×10^3). Electronic spectroscopic data in MeOH (nm, $M^{-1}cm^{-1}$): 270 (6.2×10^3), 320 (1.2×10^3), and 430 (1.6×10^3). Electronic spectroscopic data in MeCN (nm, $M^{-1}cm^{-1}$): 270 (5.5×10^3), 330 (1.3×10^3), and 450 (1.6×10^3).

2.3. Synthesis of *trans*(Cl)-[$RuCl_2$(dmso-*S*)$_2$(Hpic)]·H_2O (**2**·H_2O)

A solution of Hpic (68 mg, 0.50 mmol) in ethanol (EtOH, 10 mL) was added to a solution of *trans*(Cl)-[$RuCl_2$(dmso-*S*)$_4$] (0.25 g, 0.50 mmol) in H_2O (10 mL). The resulting solution was stirred for 3 h at room temperature and evaporated to approximately 1 mL in a vacuum. Solutions of EtOH (4 mL) followed by diethyl ether (40 mL) were added to the yellow solution, yielding an orange precipitate, **2**·H_2O. After cooling in a refrigerator (approximately 280 K) for over 12 h, the orange precipitate was washed several times by decantation with a small amount of diethyl ether, collected by filtration, washed with diethyl ether, and dried *in vacuo* (0.19 g, 82%). Orange crystals suitable for X-ray crystallography were obtained by the vapor diffusion of diethyl ether into an ethanol solution of **2**·H_2O. Analytical calculations for $RuCl_2C_{10}NS_2O_4H_{17}$·$H_2O$: C, 25.59; H, 4.08; and N, 2.98%. Observed: C, 25.57; H, 4.11; and N, 3.04%. ^{1}H NMR (270 MHz, DMSO-d_6) $\delta = 10.14$ (1H, d, 3 $J = 5.5$ Hz, H-6), 7.95 (2H, m, H-3 and H-4), 7.64 (1H, dd, 3 $J = 5.5$ and 6.9 Hz, H-5), 3.30 (6H, s, dmso), and 3.24 (6H, s, dmso). Electronic spectroscopic data in H_2O (nm, $M^{-1}cm^{-1}$): 260 (5.5×10^3), 310 (1.6×10^3), and 353 (1.9×10^3). Electronic spectroscopic data in MeOH (nm, $M^{-1}cm^{-1}$): 270 (4.0×10^3), 320 (1.5×10^3), and 370 (1.6×10^3).

Table 2
Selected bond lengths (Å), angles (deg), and dihedral angles (deg) of **1**·0·25H_2O and **2**·H_2O.

	1·0·25H_2O	**2**·H_2O
Ru1–Cl1	2.3948(4)	2.4141(4)
Ru1–Cl2	2.3920(4)	2.3883(4)
Ru1–S1	2.2540(4)	2.2446(4)
Ru1–S2	2.2176(4)	2.2268(4)
Ru1–O1	2.1367(11)	2.1343(12)
Ru1–N1	2.1395(12)	2.1260(14)
O1–C6	1.2277(18)	1.239(2)
O2–C6	1.3046(18)	1.294(2)
O2–C7	1.4540(19)	—
O1–Ru1–N1	77.29(4)	77.57(5)
S1–Ru1–S2	95.005(14)	94.377(16)
S1–Ru1–O1	87.49(3)	88.89(3)
S2–Ru1–N1	100.30(3)	99.27(4)
C11–Ru1–Cl2	173.014(15)	173.359(15)
O1–C6–O2	123.70(13)	123.66(17)
O1–C6–C1	121.37(13)	119.93(15)
O2–C6–C1	114.92(13)	116.38(16)
C6–O2–C7	116.23(12)	—

3. Results and discussion

3.1. Synthesis

The synthesis routes and reactions of **1** and **2** are summarized in Scheme 1. In 1998, Alessio and coworkers reported that when *trans*(Cl)-[$RuCl_2$(dmso-*S*)$_4$] was dissolved in water at room temperature, two dmso-*S* ligands at the *cis* position were rapidly released, forming *trans*(Cl),*cis*(*S*)-[$RuCl_2$(dmso-*S*)$_2$(OH_2)$_2$] [26]. Similarly, in the present study, the yellow heterogeneous solution of *trans*(Cl)-[$RuCl_2$(dmso-*S*)$_4$] transformed to a deep-yellow homogeneous solution after gentle warming in MeOH, forming *trans*(Cl),*cis*(*S*)-[$RuCl_2$(dmso-*S*)$_2$(MeOH)$_2$]. The ^{1}H NMR spectrum of *trans*(Cl)-[$RuCl_2$(dmso-*S*)$_4$] was acquired by heating a CD_3OD solution of the specimen at 323 K for 15 min (Fig. S1). Three singlet signals were observed at 4.82, 3.31, and 2.65 ppm. The signals at 4.82 and 2.65 ppm were assigned to H_2O in CD_3OD and free DMSO that was released from Ru^{2+}, respectively. The CD_3OD signal at 3.31 ppm overlapped with that of the coordinated dmso ligands. The intensity of the coordinated dmso ligands, which was the integral of the signal of CD_3OD subtracted from that at 3.31 ppm, was equivalent to the integral intensity of free DMSO at 2.65 ppm, suggesting that two dmso ligands at the *cis* position were released from *trans*(Cl)-[$RuCl_2$(dmso-*S*)$_4$], forming *trans*(Cl),*cis*(*S*)-[$RuCl_2$(dmso-*S*)$_2$(CD_3OD)$_2$].

For the synthesis of **1**·0·25H_2O, *trans*(Cl)-[$RuCl_2$(dmso-*S*)$_4$] was heated at 323 K for 20 min in MeOH to form *trans*(Cl),*cis*(*S*)-[$RuCl_2$(dmso-*S*)$_2$(MeOH)$_2$]. As Mepic was added into the MeOH solution of the Ru(II) complex at room temperature, the yellow solution turned orange and then clear red after stirring at room temperature for 40 h. The red complex **1**·0·25H_2O was obtained from the reaction mixture with a satisfactory yield (80%).

Similarly, the aqueous solution of *trans*(Cl)-[$RuCl_2$(dmso-*S*)$_4$], which rapidly formed *trans*(Cl),*cis*(*S*)-[$RuCl_2$(dmso-*S*)$_2$(OH_2)$_2$] upon being dissolved in water, was mixed with Hpic in EtOH and stirred for 3 h at room temperature, yielding the orange complex **2**·H_2O with a yield of 82%. In both cases, the red or orange solids were obtained in high yields (>80%) by removing the solution and eliminating two dissociated DMSO molecules from the starting *trans*(Cl)-[$RuCl_2$(dmso-*S*)$_4$] complex through several decantation cycles. The resulting complexes were characterized by elemental analysis, crystal structure studies, and ^{1}H NMR spectroscopy.

3.2. Crystal structure analysis

Oak Ridge Thermal-Ellipsoid Plot Program (ORTEP) drawings of **1**·0·25H_2O and **2**·H_2O (Fig. 2) indicated that both Ru^{2+} ions exhibited a distorted octahedral geometry with *trans*(Cl) atoms and two dmso-*S* ligands at the *cis* position (*i.e.*, *trans*(Cl),*cis*(S) geometry). In **1**·0·25H_2O, the Mepic ligand coordinated as a bidentate ligand *via* the pyridyl-*N* and carbonyl-*O* atoms. In **2**·H_2O, the Hpic ligand also coordinated as neutral bidentate ligand using the pyridyl-*N* and carbonyl-*O* atoms because cations were absent; the ^{1}H NMR spectrum of **2**·H_2O indicated that the Ru ion in **2** was diamagnetic and divalent. The reaction solution containing the **2**·H_2O precipitate had only H^+ (H_3O^+) as a cation; thus, salt

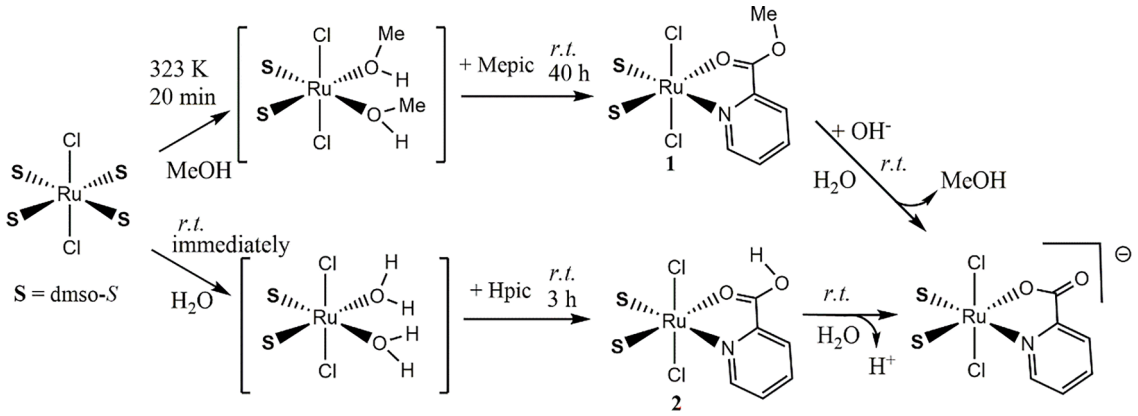

Scheme 1. Synthetic and reaction routes of 1 and 2.

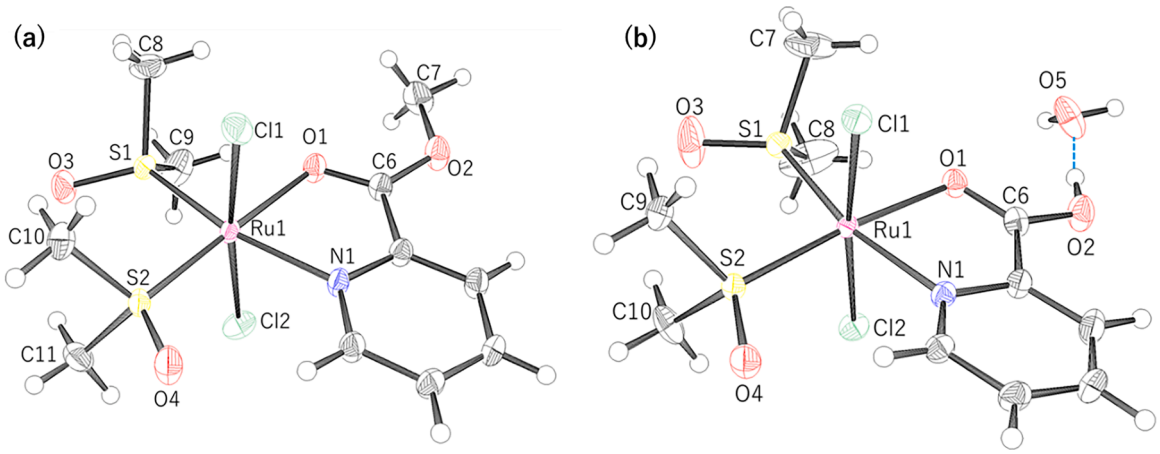

Fig. 2. ORTEP drawings of (a) **1**·0·25H_2O (without a water molecule (omitted for clarity)) and (b) **2**·H_2O. Ellipsoids are drawn at the 50% probability level.

[H_3O]*trans*(Cl)-[$RuCl_2$(dmso-*S*)$_2$(pic)] was precipitated. In the crystal, the H_3O^+ cation formed a hydrogen bond with O^- of an anionic bidentate ligand (pic^-). Although these two structures (Hpic or pic^-) could not be completely distinguished via X-ray crystallographic analyses, a difference Fourier map exhibited a hydrogen atom peak in the vicinity of a noncoordinated O atom of the ligand, and the structure of *trans*(Cl)-[$RuCl_2$(dmso)$_2$(Hpic)]·H_2O was adopted. Thus, in crystal form, **2**·H_2O should be represented as a neutral complex, *trans*(Cl)-[$RuCl_2$(dmso-*S*)$_2$(Hpic)]·H_2O. However, in solution, it might behave as a salt, [H_3O]*trans*(Cl)-[$RuCl_2$(dmso-*S*)$_2$(pic)], in which the pic^- ligand coordinates to the Ru(II) ion via pyridyl-*N* and carbonyl-O^-.

In the crystals of complex **2**, water molecules underwent hydrogen-bonding interactions with the H–O group of Hpic. A comparison of **1** and **2** suggested that **2** contained the water of crystallization instead of the Me group in **1**, allowing Hpic in **2** to retain H^+ and form H_3O^+. Moreover, water molecules underwent hydrogen-bonding interactions with the Cl1* atom in the adjacent **2** molecule and O3** atom of the dmso ligand in another adjoining **2** molecule (Fig. S2a), thereby generating two-dimensional (2D) hydrogen networks on the *bc* plane (Fig. S2b). The hydrogen-bonding parameters are summarized in Table S1.

The *trans*(Cl),*cis*(S) configuration of the two Cl and two dmso-*S* ligands in **1**·0·25H_2O and **2**·H_2O was identical to that in analogous complexes *trans*(Cl)-[$RuCl_2$(dmso-*S*)$_2$(dpk-κ^2*N,O*)] [22] and *trans*(Cl)-[$RuCl_2$(dmso-*S*)$_2$(apy)] [15]. In **1**·0·25H_2O, lengths of two Ru–Cl bonds were almost identical (2.3948(4) and 2.3920(4) Å) and similar to those in analogous complexes mono(dpk-κ^2*N,O*)Ru(II) and mono(apy)Ru(II) (2.3753(16)–2.397(1) Å). However, the Ru1–Cl1 bond (2.4141(4) Å) of **2**·H_2O was longer than another bond (2.3883(4) Å) and that of **1**·0·25H_2O. Furthermore, the length of the Ru1–S1 bond *trans* to the pyridyl-*N* atom was greater than that of the Ru1–S2 bond *trans* to the O atoms of both bidentate ligands. This tendency has also been observed in analogous complexes mono(dpk-κ^2*N,O*)Ru(II) [22] and mono(apy)Ru(II) [15].

The characteristic structural parameters were evaluated (Table 3) to investigate the effects of the *N,O*-ligand substituents in four Ru(II) complexes: **1**·0·25H_2O, **2**·H_2O, *trans*(Cl)-[$RuCl_2$(dmso-*S*)$_2$(dpk-κ^2*N,O*)] [22], and *trans*(Cl)-[$RuCl_2$(dmso-*S*)$_2$(apy)] [15]. The results showed no significant differences. However, the Ru–O bonds of **1**·0·25H_2O and **2**·H_2O were slightly longer than those of the other complexes; this tendency was not observed for the bond distance between the coordinated O and carbonyl-C atoms.

The O1–C6 bond (1.2277(18) Å) in **1**·0·25H_2O, wherein the O1 atom was coordinated to a Ru(II) ion, was clearly shorter than the O2–C6 bond (1.3046(18) Å) and similar to that in *trans*(Cl)-[$RuCl_2$(dmso-*S*)$_2$(apy)] (1.228(5) Å). These results suggest that the O1–C6 bond maintained the

Table 3
Selected bond distances (Å) and angles (°) in complexes with the substituent R of **1**·0·25H_2O and **2**·H_2O.

R =	MeO– (**1**·0·25H_2O)	HO– (**2**·H_2O)	Me– [15]	py– [22]
Ru–O	2.1367(11)	2.1343(12)	2.084(3)	2.089(2)
Ru–N	2.1395(12)	2.1260(14)	2.122(3)	2.113(2)
C = O	1.2277(18)	1.239(2)	1.228(5)	1.243(3)
O–Ru–N	77.29(4)	77.57(5)	76.59(13)	76.12(8)

O=C bond and that the C=O group was retained even after coordination to the metal ion. Moreover, the O2–C6 bond was slightly shorter than the corresponding O–C bond in pyridinecarboxylic acid ester compounds, dimethyl pyridine-2,6-dicarboxylate (Me_2pic; 1.3288(15) Å) [34] and but-2-enedioic acid bis(ethyl pyridine-2-carboxylate) (Etpic·(HOOC–CH=CH–COOH); 1.326 Å) [35]. Additionally, the O2–C7 bond (1.4549(19) Å) was significantly longer than the O2–C6 bond; however, the length of this bond was similar to those in Me_2pic (1.4510(15) Å) [32] and Etpic (1.442 Å) [35]. In **2**·H_2O, the O1–C6 bond (1.239(2) Å) was shorter than the O2–C6 bond (1.294(2) Å), and the two bond lengths were similar to the corresponding O–C bond lengths in **1**·0·25H_2O, suggesting that the O1–C6 bond preserved the O=C bond even in **2**·H_2O. In the [Ru(pic)(bpy)$_2$]Cl·CH_3CN·1·5H_2O, *cis*(*S*)-[Ru(pic)$_2$(dmso-*S*)$_2$], and *fac*(*S*)-[RuCl(pic)(dmso-*S*)$_3$] complexes, wherein the pic^- ligand acted as a mono-anionic bidentate ligand, the distance between the coordinated O^- and carbonyl-C atoms (1.280(3)–1.294(3) Å) was greater than another C–O bond length (1.218(3)–1.223(3) Å), corresponding to the C=O group [16–18]. This bond distance analysis confirmed that the bidentate ligand in **2**·H_2O was neutral Hpic. Even if **2**·H_2O was [H_3O]*trans*(Cl)-[$RuCl_2$(dmso-*S*)$_2$(pic)], H_3O^+ could form a hydrogen bond with the outside noncoordinated O atom of the bidentate ligand, delocalizing the π bond to the coordinated O and C atoms, and forming [H_3O]*trans*(Cl)-[$RuCl_2$(dmso-*S*)$_2$(pic-κ^2*N,O*)], in which the coordinated O of pic^- was neutral.

The bite angles of Mepic and Hpic in **1**·0·25H_2O and **2**·H_2O (77.29(4)° and 77.57(5)°) were similar to those in analogous complexes mono(dpk-κ^2*N,O*)Ru(II) and mono(apy)Ru(II) (76.12(8)° and 76.59(13)°). The O3 atom of the dmso-S1 ligand in **1**·0·25H_2O was oriented toward two methyl groups of the dmso-S2 ligand, and the O4 atom of the dmso-S2 ligand was directed toward the H-6 proton of the pyridyl group in Mepic. Thus, dmso-S1 bore two bulky methyl groups aimed at the slim coordinated O1 atom of Mepic, whereas dmso-S2 featured a smaller O atom of the dmso ligand directed toward the bulky pyridyl group of Mepic. Consequently, on the equatorial plane, the S1–Ru1–O1 angle was 87.49(3)°, which was close to the ideal angle of 90°, and the S1–Ru1–S2 angle (95.00(14)°) was slightly larger than 90°; moreover, the remaining S2–Ru1–N1 angle (100.30(3)°) was clearly larger than 90° The sum of the four angles around the Ru^{2+} ion within the equatorial plane was 360°, suggesting that the four coordinated atoms were in the same plane. This distribution of angles around the Ru^{2+} ion in the complex was also observed in **2**·H_2O and analogous complexes mono(dpk-κ^2*N,O*)Ru(II) and mono(apy)Ru(II). Therefore, the crystal structure analysis revealed that Mepic acted as a neutral *N,O*-ligand, and its ester group did not have a significant effect on the bonding parameters. Additionally, Hpic was confirmed to function as a neutral *N,O*-ligand depending on the reaction conditions.

3.3. IR and ^{1}H NMR spectroscopy

The IR spectra of the complexes **1**·0·25H_2O and **2**·H_2O were measured after drying them *in vacuo* for a few days and pressing them into KBr pellets (Fig. S3). The spectrum of **1**·0·25H_2O contained no ν(OH) peak for H_2O within the frequency range of 3500–3000 cm^{-1}. This suggests that the lattice water molecules were removed by drying *in vacuo*. In contrast, in the spectrum of **2**·H_2O, a strong band was observed at 3355 cm^{-1}, despite similar drying conditions. This indicates that the lattice water molecules in **2**·H_2O remained after drying, likely because of strong hydrogen-bonding interactions between the lattice water molecules and Ru(II) complex. In addition, two broad bands associated with lattice water were observed at 2250 and 1900 cm^{-1} (the band at 2250 cm^{-1} appears to be split in two, possibly because of the influence of CO_2 absorption). These broad bands are similar to those in the IR spectrum of free Hpic (2607 and 2152 cm^{-1}), which resulted from absorption by the OH group of the carboxyl group with hydrogen bonding interactions [36].

The three broad bands at 3355, 2250, and 1900 cm^{-1} in the spectrum of **2**·H_2O were further studied by comparing their shifts to those recorded for H_3O^+. H_3O^+, which has C_{3v} symmetry, has four typical IR frequencies, ν_n (n = 1–4). Vibration bands ν_1 (ν_s(OH)) and ν_3 (ν_d(OH)) usually overlap at 3600–3200 cm^{-1}, whereas ν_4 (δ_d(HOH)) and ν_2 (δ_s(HOH)) appear at 1700–1600 and 1200–1000 cm^{-1}, respectively [37, 38]. In contrast, when bound in crystals that contain strong hydrogen-bonding interactions, such as H_3O^+–crown ether compounds, the hydrogen bonds between H_3O^+ and the crown ether (of which there are three between the three hydrogen atoms of H_3O^+ and the three O atoms of the crown ether) produce an absorption band at 2400–2300 cm^{-1} [39]. This indicates that the ν(OH) band of H_3O^+ shifts to a lower energy when strong hydrogen bonds are formed. Thus, if the broad band at 2250 cm^{-1} in the spectrum of **2**·H_2O could be assigned to the ν(OH) of H_3O^+ with hydrogen bonds, no strong ν(OH) band for H_2O would be observed at 3355 cm^{-1}. This inconsistency suggests that the proton is retained on the outer noncoordinated O atom of the chelate ligand in **2** and forms the OH group of the Hpic ligand as observed in the crystal structure of **2**·H_2O. Consequently, the strong band at 3355 cm^{-1} was assigned to lattice water, and the remaining two broad bands were associated with the ν(OH) of the coordinated Hpic ligand with a hydrogen-bonding interaction with the lattice water.

As regards the dried sample of **1**, the peaks at 1650 and 1363 cm^{-1} were assigned to the asymmetric stretching (ν_a(COO)) and symmetric stretching (ν_s(COO)) of coordinated Mepic, respectively. These peaks were clearly shifted compared to those of free Mepic (1730 and 1310 cm^{-1}, respectively) [40]. **2**·H_2O produced peaks at similar positions of 1636 and 1340 cm^{-1}, assigned to ν_a(COO) and ν_s(COO), respectively. These values were shifted slightly from the corresponding values for *fac*(*S*)-[RuCl(dmso-*S*)$_3$(pic)] (ν_a(COO) = 1668 cm^{-1} and ν_s(COO) = 1334 cm^{-1}) [18], which contains the coordinated O^- of the pic^- ligand.

The ^{1}H NMR spectrum of **1** in acetone-d_6 (Fig. 3) showed four signals with 1H intensities in the aromatic region, a singlet of 3H at 4.41 ppm, and two singlets of 6H at 3.45 and 3.43 ppm. The signal intensity data implied that **1** possessed one Mepic ligand and two dmso ligands. Moreover, the spectral pattern of **1** indicated that the two methyl groups of each of the two dmso ligands were equivalent, suggesting that the two Ru–S bonds rotated in solution. The aromatic signals were assigned based on their coupling constants [30]. Similar signal patterns were observed in the ^{1}H NMR spectrum of **1** in DMSO-d_6 (Fig. S4a). However, after the NMR sample of **1** was incubated for 2–24 h at room temperature, small signals matching those of free Mepic and free DMSO were present (Figs. S4b–d). This result indicated that coordinated hemilabile Mepic thermally dissociated from the Ru(II) ion in the DMSO-d_6 solution, forming *trans*(Cl)-[$RuCl_2$(dmso)$_2$(dmso-d_6)$_2$], in which the coordinated dmso-*S* ligand was easily exchanged with the DMSO-d_6 solvent to form [$RuCl_2$(dmso-d_6)$_4$], owing to the steric hindrance between the four dmso-*S* ligands in the equatorial plane [26].

In contrast, **2**·H_2O was inert in DMSO. The ^{1}H NMR spectrum of **2**·H_2O in DMSO-d_6 (Fig. 4) showed four signals with ^{1}H band intensities in the aromatic region and two singlets with intensities of 6H. These signals were assigned to a coordinated pyridyl group and two coordinated dmso-*S* ligands in **2**. No signal was observed for the HO group of coordinated Hpic. Moreover, the signal of water in DMSO-d_6 emerged at 5.2 ppm; however, this signal typically appears at 3.3 ppm. This shift was caused by the formation of H_3O^+ with an acidic proton (H^+) that was released from the coordinated Hpic in DMSO-d_6 and with water in the solvent. The ^{1}H NMR spectrum remained identical even after the NMR sample of **2**·H_2O was incubated for a day at 323 K (Fig. S5). Although crystal structure analysis indicated that the Hpic ligand in **2** was coordinated to a Ru(II) ion *via* pyridyl-*N* and carbonyl-*O* atoms, thermal decomposition in DMSO was not observed. In solution, the H^+ ion of Hpic was released to form *trans*(Cl)-[$RuCl_2$(dmso-*S*)$_2$(pic-κ^2*N,O*$^-$)]$^-$, in which the coordinated O atom was negatively charged. Therefore, **2** was inert despite having a hemilabile *N,O*-ligand, owing to the deprotonation of the coordinated Hpic to become a negative bidentate ligand.

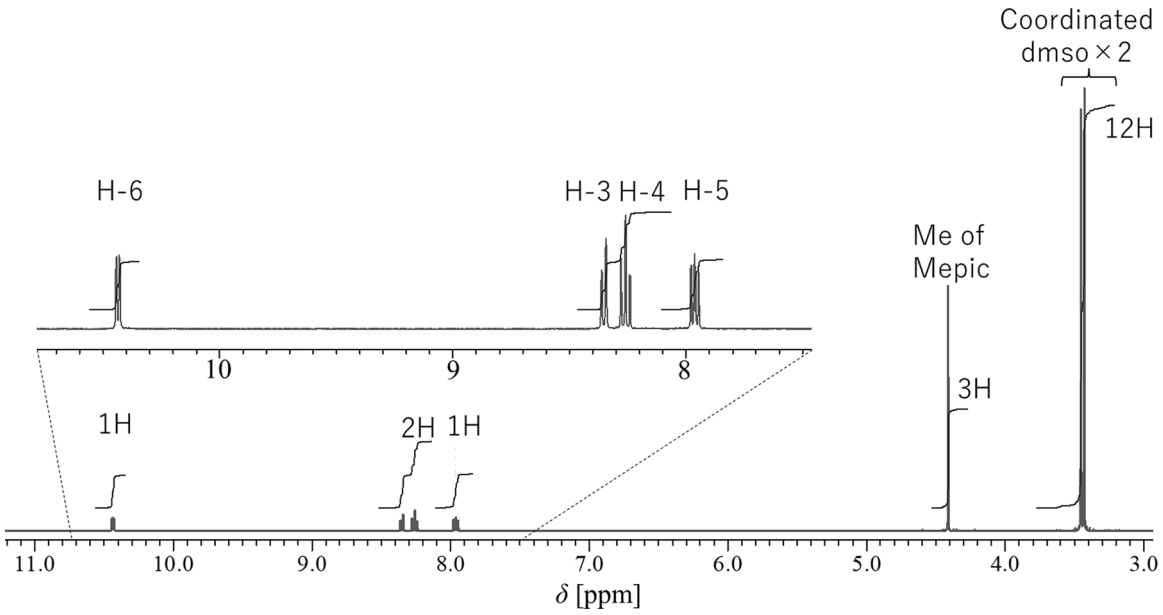

Fig. 3. ^{1}H NMR spectrum of **1**·0·25H_2O in acetone-d_6 (300 MHz).

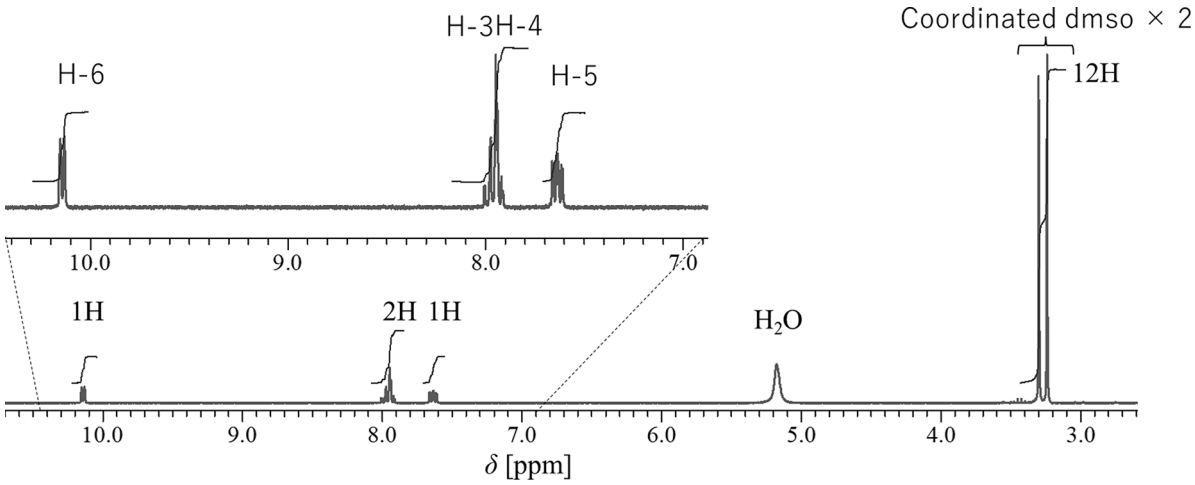

Fig. 4. ^{1}H NMR spectrum of **2**·H_2O in DMSO-d_6 (270 MHz).

3.4. Chemical behavior in aqueous solutions

The orange complex **2**·H_2O was dissolved in water, and the resulting aqueous solution became slightly acidic (pH 4) and yellow; this result suggested that the proton of the carboxylic group was released in water to form *trans*(Cl)-[$RuCl_2$(dmso-*S*)$_2$(pic-κ^2*N,O*$^-$)]$^-$. The ^{1}H NMR spectrum of **2**·H_2O in D_2O was identical to that of the neutralized D_2O solution of **2**·H_2O with NaOH(aq) (Fig. S6). Additionally, the ^{1}H NMR spectrum of **2**·H_2O in D_2O after heating at 323 K for 3 h was consistent with that of the unheated sample (Fig. S7). This result substantiated that the pic$^-$ component of the complex was coordinated to a Ru^{2+} ion *via* pyridyl-*N* and negatively charged O^- atoms, thereby providing electrostatic assistance for binding to the Ru^{2+} ion to form *trans*(Cl)-[$RuCl_2$(dmso-*S*)$_2$(pic-κ^2*N,O*$^-$)]$^-$.

In water, complex **2** was inert and existed as *trans*(Cl)-[$RuCl_2$(dmso-*S*)$_2$(pic-κ^2*N,O*$^-$)]$^-$, whereas complex **1** was labile. In the ^{1}H NMR spectrum of **1**·0·25H_2O in D_2O, the singlet signal of the Me group of the coordinated Mepic ligand appeared at 4.37 ppm. After heating the solution of **1**·0·25H_2O in D_2O at 323 K for a few hours, the resulting ^{1}H NMR spectrum differed from that of the unheated counterpart (Fig. S8). The signals of **1** decreased in intensity, and two new H-6 signals of the pyridyl group appeared in the aromatic region. The new signal at 3.34 ppm was assigned to the Me group of free MeOH. The appearance of the MeOH signal implies that a hydrolysis reaction occurred with the coordinated Mepic to form *trans*(Cl)-[$RuCl_2$(dmso-*S*)$_2$(pic-κ^2*N,O*$^-$)]$^-$, however, both of new H-6 signals in Fig. S8c did not match that of **2**·H_2O. Thus, new thermal products would be complexes with a pic$^-$, which was formed from Mepic by hydrolysis, and lose the monodentate a Cl^- or dmso ligand by thermal decomposition. But, both of free Mepic and **2**·H_2O were inert in water (Fig. S9). Consequently, these results suggest that Mepic was somewhat labilized by coordination with Ru(II) ions. Additionally, the dissociation of the monodentate ligands occurs simultaneously with the hydrolysis of the coordinating Mepic. The fact, that **1**·0·25H_2O is labile in water, means that it is reasonable to use MeOH as the solvent for synthesis of **1**; however, the hydrolysis compound of *trans*(Cl)-[$RuCl_2$(dmso-*S*)$_4$] in water has been used as a precursor to synthesize *trans*(Cl)-[$RuCl_2$(dmso-*S*)$_2$(L-L)] complexes [22, 41–43].

^{1}H NMR showed that free Mepic was inert in water; however, the reaction of Mepic with OH^- in water quickly afforded MeOH and pic$^-$

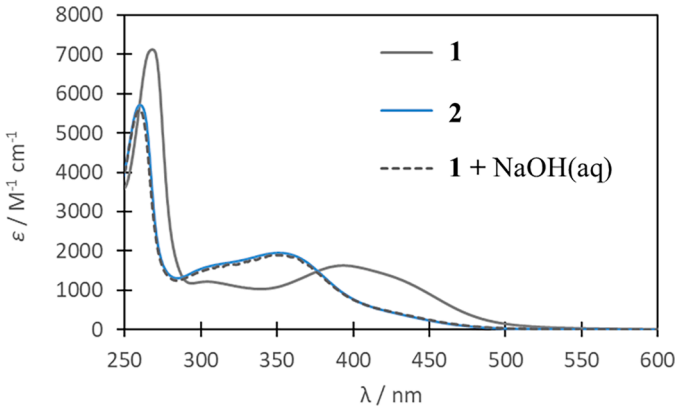

Fig. 5. Absorption spectra of **1**·0·25H_2O and **2**·H_2O in H_2O at 298 K. The dashed line is the absorption spectrum of a solution containing **1**·0·25H_2O and an equal amount of NaOH.

(Fig. S10). Similarly, after NaOH(aq) was added to a D_2O solution of **1** in an amount equimolar to **1** without heating, the resulting spectrum in the aromatic region was identical to that of **2** in D_2O, and **2** became *trans*(Cl)-[$RuCl_2$(dmso-*S*)$_2$(pic-κ^2*N,O*$^-$)]$^-$ in D_2O. Thus, the reaction of **1** with OH^- in water selectively produced *trans*(Cl)-[$RuCl_2$(dmso-*S*)$_2$(pic-κ^2*N,O*$^-$)]$^-$ without the dissociation of monodentate ligands; moreover, in the aliphatic region, the signal at 4.37 ppm—corresponding to the Me group of Mepic—disappeared and a new free-MeOH-associated singlet signal with the intensities of 3H appeared at 3.34 ppm (Fig. S10b). These findings were corroborated by the absorption spectra of **1**·0·25H_2O and **2**·H_2O in water (Fig. 5). The addition of an aqueous NaOH solution to the orange **1**·0·25H_2O solution at ambient temperature resulted in a yellow solution. Notably, the absorption spectrum of the yellow solution was identical to that of **2**·H_2O. Adding aqueous trifluoromethanesulfonic acid (HOTf(aq)) to the aqueous solution of **2**·H_2O (at twice the molar amount of **2**·H_2O) resulted in an ^{1}H NMR spectrum that was identical to that of **2**·H_2O (Fig. S12). Overall, the ^{1}H NMR and UV–Vis spectroscopic data suggest that the OH^- ions in solution selectively reacted with the coordinated Mepic in **1** to cleave the ester bond, whereas the reverse reaction of H^+ dissociation was not observed, even when excess H^+ was added to the aqueous solution of **2**·H_2O.

4. Conclusion

A Ru(II) complex with Mepic, **1**·0·25H_2O, and the corresponding complex with Hpic, **2**·H_2O, were synthesized and their crystal structures and behaviors in DMSO and water solutions were investigated. The crystal structure analysis of the two complexes indicated that the structural parameters of the *trans*(Cl)-$RuCl_2$(dmso-*S*)$_2$ geometry were almost identical, and that Mepic and Hpic acted as neutral bidentate *N,O*-ligands. Moreover, the crystals of **2**·H_2O had a water molecule in a position similar to that of the Me group in **1**·0·25H_2O. Evidently, water was important for the Hpic ligand in **2**·H_2O to retain H^+ during crystallization. Notably, H^+ was released from Hpic in the **2**·H_2O solution to form the anionic *trans*(Cl)-[$RuCl_2$(dmso-*S*)$_2$(pic-κ^2*N,O*$^-$)]$^-$ complex. Thus, the structure of **2**·H_2O was *trans*(Cl)-[$RuCl_2$(dmso-*S*)$_2$(Hpic)]·H_2O in the crystal form, and [H_3O]*trans*(Cl)-[$RuCl_2$(dmso-*S*)$_2$(pic)] in solution. In a DMSO solution, **1** was labile owing to the presence of the neutral hemilabile *N,O*-ligand; however, **2** was inert because Hpic behaved as a negative bidentate pic$^-$ ligand, (pic-κ^2*N,O*$^-$)$^-$. Although free Mepic was inert in water, after heating **1**·0·25H_2O in water, the coordinated Mepic underwent a slow decomposition reaction to form MeOH and some Ru(II)-pic$^-$ complexes, in which monodentate ligands were dissociated by thermal hydrolysis. When OH^- ions were added to an aqueous solution of **1**, the decomposition of coordinated Mepic proceeded selectively and rapidly, forming the anionic *trans*(Cl)-[$RuCl_2$(dmso-*S*)$_2$(pic-κ^2*N,O*$^-$)]$^-$ complex and free MeOH molecules, without dissociation of the monodentate ligands. This study promotes the understanding of the behavior of Ru(II) complexes in different environments, providing valuable information for their potential applications in catalysis, drug development, material science, and coordination chemistry.

CRediT authorship contribution statement

Mari Toyama: Writing – review & editing, Writing – original draft, Project administration, Investigation, Funding acquisition, Conceptualization. **Yuto Onishi:** Investigation. **Nobuyoshi Tanaka:** Investigation. **Noriharu Nagao:** Writing – review & editing, Validation.

Declaration of competing interest

The authors declare that they have no known competing financial interests or personal relationships that could have appeared to influence the work reported in this paper.

Data availability

Data will be provided as Supporting Information (PDF).

Acknowledgements

This study was financially supported by the Fundamental Electronics Research Institute (FERI), Osaka Electro-Communication University, Japan. The authors are also grateful to Professor K. Katagiri at Konan University, Japan, for assistance with the ^{1}H NMR spectroscopy measurements conducted at 300 MHz. We would like to thank Editage (www.editage.jp) for English language editing.

Supplementary materials

Supplementary material associated with this article can be found, in the online version, at doi:10.1016/j.molstruc.2024.139964.

References

[1] R.S. Mane, T. Sasaki, B.M. Bhanage, Silica supported palladium-phosphine as a reusable catalyst for alkoxycarbonylation and aminocarbonylation of aryl and heteroaryl iodides, RSC Adv. 5 (2015) 94776–94785, https://doi.org/10.1039/C5RA18692G.

[2] C.H. Tsai, M. Xu, P. Kunal, B.G. Trewyn, Aerobic oxidative esterification of primary alcohols over Pd-Au bimetallic catalysts supported on mesoporous silica nanoparticles, Catal. Today. 306 (2018) 81–88, https://doi.org/10.1016/j.cattod.2017.01.046.

[3] H. Yu, J. Wang, Z. Wu, Q. Zhao, D. Dan, S. Han, J. Tang, Y. Wei, Aldehydes as potential acylating reagents for oxidative esterification by inorganic ligand-supported iron catalysis, Green Chem. 21 (2019) 4550–4554, https://doi.org/10.1039/C9GC02053E.

[4] Z. Guo, E.D. Dowdy, W.S. Li, R. Polniaszek, E. Delaney, A novel method for the mild and selective amidation of diesters and the amidation of monoesters, Tetrahedron Lett. 42 (2001) 1843–1845, https://doi.org/10.1016/S0040-4039(01)00079-X.

[5] Q. You, D.B. Collum, Carbon–nitrogen bond formation using sodium hexamethyldisilazide: solvent-dependent reactivities and mechanisms, J. Am. Chem. Soc. 145 (2023) 23568–23584, https://doi.org/10.1021/jacs.3c07317.

[6] C. Yuan, J. Yan, C. Song, F. Yang, C. Li, C. Wang, H. Su, W. Chen, L. Wang, Z. Wang, S. Qian, L. Yang, Discovery of [1,2,4]triazole derivatives as new metallo-β-lactamase inhibitors, Molecules 25 (2020) 56, https://doi.org/10.3390/molecules25010056.

[7] M.S. Kim, L.A. Buisson, D.A. Heathcote, H. Hu, D.C. Braddock, A.G.M. Barrett, P. G. Ashton-Rickardt, J.P. Snyder, Approaches to design non-covalent inhibitors for human granzyme B (hGrB), Org. Biomol. Chem. 12 (2014) 8952–8965, https://doi.org/10.1039/C4OB01874E.

[8] P. Gonzáles-Duarte, R. March, J. Pons, W. Clegg, L. Cucurull-Sànchez, A. Álvarez-Larena, J.F. Piniella, Synthesis and x-ray structure of zinc(II) derivatives of esters of 2-pyridinecarboxylic acid, Polyhedron 15 (1996) 2747–2754, https://doi.org/10.1016/0277-5387(95)00549-8.

[9] R. March, J. Pons, J. Ros, W. Clegg, A. Álvarez-Larena, J.F. Piniella, J. Sanz, Reactivity of 2-pyridinecarboxylic esters with cadmium (II) halides: study of ^{113}Cd NMR solid state spectra and crystal structures of hexacoordinated complexes $[CdI_2(C_5H_4NCOOMe)_2]$ and $[CdI_2(C_5H_4NCOOPr^n)_2]$, Inorg. Chem. 42 (2003) 7403–7409, https://doi.org/10.1021/ic0206387.

[10] D.Hanh Nguyen, N. Lassauque, L. Vendier, S. Mallet-Ladeira, C.Le Berre, P. Serp, P. Kalck, Reductive elimination of anhydrides from anionic iodo acetyl carboxylato rhodium complexes, Eur. J. Inorg. Chem. 2014 (2014) 326–336, https://doi.org/10.1002/ejic.201300933.

[11] C. Binnani, R.K. Rai, D. Tyagi, S.M. Mobin, S.K. Singh, Ligand-tuned C–H bond activation/arylation of 2-arylpyridines over pyridine-based *N, O/N, N* ligated ruthenium–arene complexes, Eur. J. Inorg. Chem. 2018 (2018) 1435–1445, https://doi.org/10.1002/ejic.201701446.

[12] B.S. Tovrog, S.E. Diamond, F. Mares, Oxidation of ruthenium coordinated alcohols by molecular oxygen to ketones and hydrogen peroxide, J. Am. Chem. Soc. 101 (1979) 5067–5069, https://doi.org/10.1021/ja00511a048.

[13] A.S.A.T. de Paula, B.E. Mann, E. Tfouni, Properties and one-step synthesis of (2-acetylpyridine)tetraammineruthenium(II), $[Ru^{II}(2\text{-acpy})(NH_3)_4]^{2+}$ and tetraammine(2-benzoylpyridine)ruthenium(II), $[Ru^{II}(NH_3)_4(2\text{-bzpy})]^{2+}$: redox potentials, UV–Vis and NMR spectra, Polyhedron 18 (1999) 2017–2026, https://doi.org/10.1016/S0277-5387(99)00076-5.

[14] D. Zuccaccia, G. Bellachioma, G. Cardaci, C. Zuccaccia, A. Macchioni, Aggregation Tendency and Reactivity Toward AgX of Cationic Half-Sandwich ruthenium(II) Complexes Bearing Neutral N,O-ligands, 16, Dalton Trans, 2006, pp. 1963–1971, https://doi.org/10.1039/B514269E.

[15] S. Pal, S. Pal, *trans*-(2-Acetylpyridine-κ^2*N,O*)dichlorobis(dimethyl sulfoxide-κ*S*) ruthenium(II), Acta Crystallogr. C. 58 (2002) m273–m274, https://doi.org/10.1107/S0108270102003797.

[16] M. Toyama, T. Nakayasu, N. Nagao, Crystal structure of (2-picolinato)bis(2,2′-bipyridine)ruthenium(II) chloride, X-ray Struct, Anal. Online 33 (2017) 11–13, https://doi.org/10.2116/xraystruct.33.11.

[17] A.A. Rachford, J.L. Petersen, J.J. Rack, Phototriggered Sulfoxide Isomerization in $[Ru(pic)_2(dmso)_2]$, 30, Dalton Trans, 2007, pp. 3245–3251, https://doi.org/10.1039/B704205A.

[18] I. Bratsos, C. Simonin, E. Zangrando, T. Gianferrara, A. Bergamo, E. Alessio, New Half Sandwich-Type Ru(II) Coordination Compounds Characterized by the *fac*-Ru(dmso-S)$_3$ fragment: Influence of the Face-Capping Group On the Chemical Behavior and *in Vitro* Anticancer Activity, 40, Dalton Trans, 2011, pp. 9533–9543, https://doi.org/10.1039/C1DT11043H.

[19] K.K. Bania, R.C. Deka, Zeolite-Y encapsulated metal picolinato complexes as catalyst for oxidation of phenol with hydrogen peroxide, J. Phys. Chem. C. 117 (2013) 11663–11678, https://doi.org/10.1021/jp402439x.

[20] T. Koleša-Dobravc, K. Maejima, Y. Yoshikawa, A. Meden, H. Yasui, F. Perdih, Bis(picolinato) complexes of vanadium and zinc as potential antidiabetic agents: synthesis, structural elucidation and *in vitro* insulin-mimetic activity study, New J. Chem. 42 (2018) 3619–3632, https://doi.org/10.1039/C7NJ04189F.

[21] G. Ferraro, N. Demitri, L. Vitale, G. Sciortino, D. Sanna, V. Ugone, E. Garribba, A. Merlino, Spectroscopic/computational characterization and the X-ray structure of the adduct of the $V^{IV}O$–picolinato complex with RNase A, Inorg. Chem. 60 (2021) 19098–19109, https://doi.org/10.1021/acs.inorgchem.1c02912.

[22] M. Toyama, M. Nakahara, N. Nagao, Syntheses, crystal structures, and conversion of three linkage isomers of di-2-pyridyl ketone in dichlorobis(dimethylsulfoxide-*S*) ruthenium(II) and chlorobis(dimethylsulfoxide-*S*)ruthenium(II) complexes: $[RuCl_2(dpk\text{-}\kappa^2N,O)(dmso\text{-}S)_2]$, $[RuCl_2(dpk\text{-}\kappa^2N,N')(dmso\text{-}S)_2]$, and $[RuCl(dpk\text{-}OH\text{-}\kappa^3N,O,N')(dmso\text{-}S)_2]$, Bull. Chem. Soc. Jpn. 80 (2007) 937–950, https://doi.org/10.1246/bcsj.80.937.

[23] M. Toyama, N. Nagao, Crystal structure of *cis*(S),*trans*(O,N_{bpy})-(2,2′-bipyridyl-κ^2*N,N′*)bis(dimethyl sulfoxide-κ*S*)[phenyl(pyridin-2-yl)methanone-κ^2*N,O*]ruthenium (II) bis(trifluoromethanesulfonate), Acta Crystallogr 78 (2022) 1189–1193, https://doi.org/10.1107/S2056989022010258. E.

[24] M. Toyama, Y. Fujii, M. Endo, Bis-heteroleptic ruthenium(II) complex with 2-picolinamide: synthesis, crystal structures, and spectroscopic study for anion recognition using the amide group, Inorg. Chim. Acta. 486 (2019) 304–313, https://doi.org/10.1016/j.ica.2018.10.060.

[25] M. Toyama, T. Hasegawa, N. Nagao, Colorimetric fluoride detection in dimethyl sulfoxide using a heteroleptic ruthenium(II) complex with amino and amide groups: x-ray crystallographic and spectroscopic analyses, RSC Adv 12 (2022) 25227–25239, https://doi.org/10.1039/D2RA03593F.

[26] E. Alessio, G. Mestroni, G. Nardin, W.M. Attia, M. Calligaris, G. Sava, S. Zorzet, Cis- and trans-dihalotetrakis(dimethyl sulfoxide)ruthenium(II) complexes (RuX2 (DMSO)4; X = Cl, Br): synthesis, structure, and antitumor activity, Inorg. Chem 27 (1988) 4099–4106, https://doi.org/10.1021/ic00296a006.

[27] S. Roeser, S. Maji, J. Benet-Buchholz, J. Pons, A. Llobet, Synthesis, characterization, reactivity, and linkage isomerization of $Ru(Cl)_2(L)(DMSO)_2$ complexes, Eur. J. Inorg. Chem. 2013 (2013) 232–240, https://doi.org/10.1002/ejic.201200809.

[28] E. Alessio, E. Iengo, S. Geremia, M. Calligaris, New geometry and linkage isomers of the Ru(II) precursor *cis,cis,trans*-$RuCl_2$(dmso-S)$_2$(dmso-O)(CO): a spectroscopic and structural investigation, Inorg. Chim. Acta 344 (2003) 183–189, https://doi.org/10.1016/S0020-1693(02)01318-X.

[29] H.E. Gottlieb, V. Kotlyar, A. Nudelman, NMR chemical shifts of common laboratory Solvents as Trace Impurities, J. Org. Chem. 62 (1997) 7512–7515, https://doi.org/10.1021/jo971176v.

[30] N. Nagao, M. Mukaida, S. Tachiyashiki, K. Mizumachi, Nuclear magnetic resonance studies on the structure of ruthenium(II) complexes of di-2-pyridylamine in DMSO solution, Bull. Chem. Soc. Jpn. 67 (1994) 1802–1808, https://doi.org/10.1246/bcsj.67.1802.

[31] M.C. Burla, R. Caliandro, B. Carrozzini, G.L. Cascarano, C. Cuocci, C. Giacovazzo, M. Mallamo, A. Mazzone, G. Polidori, Crystal structure determination and refinement *via SIR2014*, J. Appl. Crystallogr. 48 (2015) 306–309, https://doi.org/10.1107/S1600576715001132.

[32] CrystalStructure Analysis Package, Rigaku Corporation (2000-15), Tokyo-8666, Japan, 2014, p. 196. https://www.rigaku.com/downloads/software/crystalstructure/.

[33] G.M. Sheldrick, A short history of *SHELX*, Acta Crystallogr. A. 64 (2008) 112–122, https://doi.org/10.1107/S0108767307043930.

[34] J.Y. Huang, W. Xu, Dimethyl pyridine-2,6-dicarboxylate, Acta Crystallogr. E 62 (2006) o2653–o2654, https://doi.org/10.1107/S160053680601988X.

[35] S. Selyani, M. Dinçer, Salt and co-crystal formation from the reaction of fumaric acid with different N-heterocyclic compounds: experimental and DFT study, Mol. Cryst. Liq. Cryst. 666 (2018) 65–78, https://doi.org/10.1080/15421406.2018.1512451.

[36] D. Li, G.Q. Zhong, Synthesis, Crystal Structure, and Thermal Decomposition of the Cobalt(II) Complex with 2-Picolinic Acid, Sci. World J. 1 (2014) 641606, https://doi.org/10.1155/2014/641608.

[37] K. Nakamoto, Infrared and Raman Spectra of Inorganic and Coordination Compounds Part A, 5th ed., John Wiley & Sons, 1997, pp. 173–179.

[38] E.S. Stoyanov, Composition structure and IR spectra peculiarities of proton hydratosolvates $H^+(H_2O)_NL_p$ formed in tributylphosphate solution of strong acid $HFeCl_4$, J. Chem. Soc., Faraday Trans. 93 (1997) 4165–4175, https://doi.org/10.1039/A702704D.

[39] W.J. Wang, B. Chen, P. Zheng, B. Wang, M. Wang, Solvent-extraction complex of uranium(VI) with *cis,syn,cis*-dicyclohexano-18-crown-6, Inorg. Chim. Acta 117 (1986) 81–82, https://doi.org/10.1016/S0020-1693(00)88071-8.

[40] A.R. Katritzky, A.M. Monro, J.A.T. Beard, D.P. Dearnaley, N.J. Earl, *N*-oxides and related compounds. Part XII. Infrared spectra of some carbonyl compounds, J. Chem. Soc. (1958) 2182–2191, https://doi.org/10.1039/JR9580002182.

[41] M. Toyama, K. Inoue, S. Iwamatsu, N. Nagao, Syntheses and crystal structures of mono(2,2′-bipyridine)dichlorobis(dimethylsulfoxide-*S*)ruthenium(II) complexes, $[RuCl_2(bpy)(dmso\text{-}S)_2]$, Bull. Chem. Soc. Jpn. 79 (2006) 1525–1534, https://doi.org/10.1246/bcsj.79.1525.

[42] M. Toyama, R. Suganoya, D. Tsuduura, N. Nagao, Syntheses and crystal structures of mono(di-2-pyridylamine)chloro(dimethylsulfoxide-*S*)ruthenium(II) complexes $[RuCl_2(Hdpa)(dmso\text{-}S)_2]$ and $[RuCl(Hdpa)(dmso\text{-}O)(dmso\text{-}S)_2](OTf)$, Bull. Chem. Soc. Jpn. 80 (2007) 922–936, https://doi.org/10.1246/bcsj.80.922.

[43] M. Toyama, S. Iwatsuki, N. Nagao, Crystal structure of *trans*(Cl),*cis*(S)-dichlorobis(dimethyl sulfoxide-*S*)(*N,N,N′,N′*-tetramethylethylenediamine)ruthenium(II), X-ray Struct. Anal. Online 32 (2016) 25–26, https://doi.org/10.2116/xraystruct.32.25.